

Visualizing the melting processes in ultrashort intense laser triggered gold mesh with high energy electron radiography

Zheng Zhou,¹ Yu Fang,¹ Han Chen,¹ Yipeng Wu,¹ Yingchao Du,^{1, a)} Zimin Zhang,² Yongtao Zhao,^{3, 2} Ming Li,⁴ Chuanxiang Tang,¹ and Wenhui Huang¹

¹⁾*Department of Engineering Physics, Tsinghua University, Beijing 100084, China*

²⁾*Institute of Modern Physics, Chinese Academy of Sciences, Lanzhou 730000, China*

³⁾*Xian Jiaotong University, Xian 710049, China*

⁴⁾*Institute of Applied Electronics, CAEP, Mianyang 621900, China*

(Dated: 17 November 2021)

High energy electron radiography (HEER) is a promising tool for high energy density physics diagnostics, apart from other tools like X/ γ ray shadowgraphy and high energy proton radiography. Impressive progresses have been made in development and application of HEER in past few years, and proved its potentials for high-resolution imaging of static opaque objects. By taking advantages of short pulse duration and tunable time structure of high energy electron probes, time-resolved imaging measurement of high energy density gold irradiated by ultrashort intense lasers has been performed. Phenomena of different time periods from picosecond to microsecond have been observed, thus proving feasibilities of this technique for imaging of static and dynamic objects.

I. INTRODUCTION

High energy density physics (HEDP) is the study of matters under extreme conditions, often designated by > 1 Mbar (100 GPa) pressure or > 100 GJ/m³ energy density¹, such as those occurring in heavy ion², laser driven fusion³ and similar processes. Under these conditions, hydrodynamic response of the matter is a high expansion velocity in the range of $\mu\text{m/ns}$, thus posing various challenges on diagnostic tools, such as high spatiotemporal resolution, high areal density resolution and a large dynamic range⁴. Charged particle radiography⁵ has been developed as a diagnostic tool for many years by Los Alamos National Laboratory⁶⁻⁸ and other institutes⁹⁻¹¹. As an alternative option to intensively studied proton radiography, high energy electron radiography (HEER)¹² has drawn considerable interest due to its potentials to provide high spatiotemporal resolution with much easier accessibility and manipulability. Recent works have improved spatial resolution of HEER to a few microns^{13,14} and applied this technique to image dynamic processes¹⁴. However, full advantages of high energy electron probes with short pulse duration and flexibly tunable time structure have not been taken yet, and this is especially true when using high brightness electron probes generated from state-of-the-art RF photo-injectors. In a common photo-injector, pulse duration of an electron bunch can be down to ps or even fs level, and synchronization between the RF and laser can be controlled to sub-ps level. Therefore, the accuracy of time-resolved imaging of dynamic process in pump-probe scheme can reach ps level, at which level some ultrafast phenomena can be observed.

In this paper, we demonstrate the use of high brightness electron probes and a compact imaging lens composed of high gradient permanent magnet quadrupoles (PMQ) to capture the entire dynamic process of laser ablation of gold mesh over a large time scale, with tens of ps- μm spatiotemporal resolution. Successful implement of dynamic high energy

^{a)}Electronic mail: dych@mail.tsinghua.edu.cn

electron radiograph, in ultra-fast intense laser pump, ps long high energy electron probe scheme, reveals its potential for direct visualization of fast dynamic phenomena in high energy density matters.

II. DYNAMIC HEER EXPERIMENT

A. experimental setup

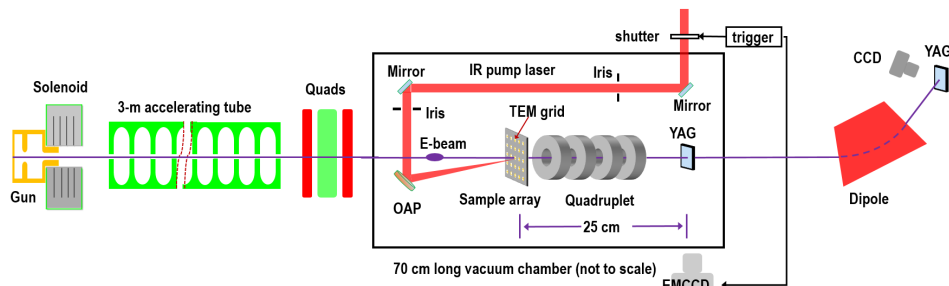


FIG. 1. Schematic of the dynamic HEER experimental layout. High brightness electron probes passing through the sample form a point-to-point, magnified image of sample with the magnetic imaging system. To image the irreversible laser ablation process, a specially designed sample holder containing numerous identical grids is mounted on a two-dimension translation stage in xy plane.

Proof-of-principle experiments of dynamic HEER were carried out at Tsinghua Thompson scattering X-ray source¹⁵ platform, which consists of a high-gradient normal-conducting RF gun working at 2.856 GHz, a 3-m long travelling wave accelerating tube and some other elements for beam control and diagnosis. A schematic layout of this experiment is shown in Fig.1. High brightness electron probes with 300 pC bunch charge, 1 mm.mrad normalized emittance, 10 ps pulse duration, 45 MeV kinetic energy and 0.1% energy spread are generated from the photo-injector. At the exit of the accelerator, an electromagnetic quadrupoles composed triplet is used to focus the beam and match it into the imaging lenses section, which is entirely installed in the vacuum chamber. Electrons passing the the sample will travel through a PMQ based Russian quadruplet (RQ) and finally form a point-to-point image of the sample on a high-resolution YAG screen. Image of the sample will be recorded by a lens-coupled CCD outside of the chamber. A dipole magnet at the end of beamline is to calibrate the kinetic energy as well as measure the energy spread of the electron probe.

TABLE I. Parameters describing the Russian quadruplet.

Name	Length	Gradient	Position
A_1	18.63 mm	-186.1T/m	0.02929 m
B_1	20.04 mm	214.2T/m	0.08366 m
B_2	20.16 mm	-209.0T/m	0.13915 m
A_2	18.63 mm	186.3T/m	0.19348 m

The RQ imaging lens is composed of two pairs of PMQs, which have found wide use in high energy particle transport¹⁶, focusing¹⁷ and imaging^{18,19}, due to their 1-2 order of magnitude higher gradients than common electromagnetic quadrupoles. Since their gradients cannot be tuned, positions of these PMQs are optimized by code COSY INFINITY²⁰. Parameters of the optimized layout of RQ are listed in Table. I. Fitness of the imaging section is verified by particle-tracking simulation using code ASTRA²¹, with both hard-edge PMQ model (same

model used in COSY INFINITY code) and measured PMQ field distribution. In Fig. 2, a point-to-point image of a 100% initial contrast sample (i.e, a standard 200 mesh hexagon TEM grid) is formed, with a magnification factor of about 1.1. The simulated imaging process matches well with experimental outcomes. Resolution of this imaging system is determined to be $15 \mu\text{m}$ by measuring the edge spread function of a bar of the grid, as shown in Fig. 3.

B. Calibration of time-of-zero

In pump-probe scheme, the first step for imaging the dynamic processes is to calibrate the time-of-zero, i.e, the beginning timestamp of laser initiated exciting of the sample. Electron deflectometry or shadowgraphy^{22,23} is a widely used technique in determination of time-of-zero in laser-pump-electron-probe experiments, where electrons will be deflected by transient electromagnetic fields induced by high power density laser illumination of a metal target. In addition, this technique is found to be a promising tool for diagnosis of transient electric and magnetic fields²⁴ and highly dense plasma evolving²⁵. However, energy of electron probes used in previous experiments is limited to tens of keV up to a few MeV, since highly energetic electrons are more difficult to deflect. Advantage of higher energy electrons is also obvious, that is they could penetrate denser plasma and detect higher electric and magnetic fields²⁴.

In this experiment, an ultra-short high power intensity pump laser of $28 (\pm 5\%)$ mJ pulse energy, 40 ± 2 fs pulse duration (full width half height) is illuminating on a small area of $< 30 \mu\text{m}$ of the gold mesh, thus the power density is about $5 \times 10^{16} \text{ W/cm}^2$. With the RQ moved off the z axis, shadowgraphs of the laser irradiated sample are obtained. At a certain delay time, for example, $T = 4.8$ ns in Fig. 4(a), beam intensity of the illuminating area drops while outer part intensity increases due to the deflection effect, thus forming a "valley-peak" intensity distribution pattern, which is very similar to those phenomena in previous experiment²⁴. Moreover, by measuring position offsets of centroid of each beamlet passing through the mesh holes with pump laser on, one can calculate the deflection angle of the electrons located in the "peak" area, which is about 1.7 mrad in maximum. By tuning the time delay between electron probe and pump laser, the lasting time of this phenomenon

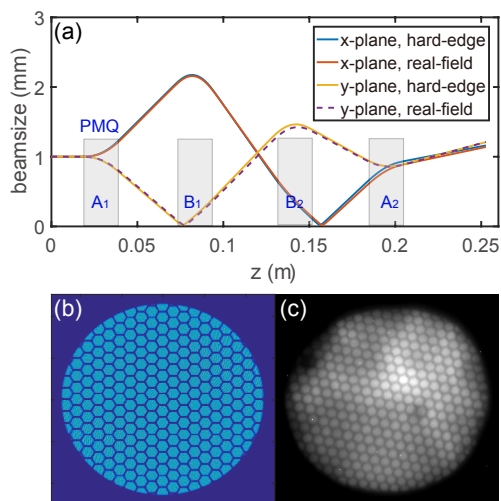


FIG. 2. (a): Simulated beam transverse envelop in imaging section. (b): simulated static image of a 200-mesh hexagon TEM grid. (c): experimental static image of a 200-mesh hexagon TEM grid.

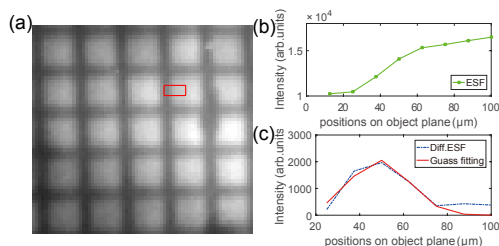


FIG. 3. (a): Image of the central part of a 200-mesh square TEM grid. (b): beam intensity distribution in x plane, i.e., edge spread function (ESF) of the grid bar in the region of interest marked by red box in (a). (c): the line spread function (differentiation of ESF) of the grid bar and its Gaussian fit plot. 1-sigma resolution is determined to be about $15 \mu\text{m}$.

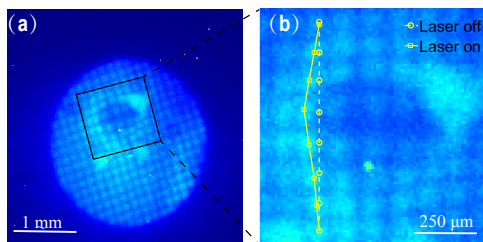


FIG. 4. (a): Electron deflection by transient electromagnetic fields at $T=4.8 \text{ ns}$. (b): zoom view of the laser illuminating area.

is determined to be approximate 8 ns.

C. Imaging the melting process

Known the time-of-zero, imaging mode was shifted from shadowgraph to radiograph mode, with RQ moved back to beam axis. Since the photo-injector is working on single pulse mode with a repetition rate of 10 Hz, the whole unrepeatable melting process can not be recorded with a single pulse. Therefore we designed a special sample holder containing numerous identical gold meshes, and by carefully varying time delay over a large dynamic scale, we can acquire a sequence of images of the sample at different time to piece together an entire movie of the melting process, as shown in Fig. 5.

By analysing evolution of the beam intensity as well as the surface profile of the sample, the whole melting process can be divided into three different phases. In the first phase lasting from the beginning to about 10 ns, radiographs of the phase are almost same to the background-shots, unlike the obvious deflection observed in shadowgraph mode. This can be explained by the fact that the relatively small scatter angles imprinted on electrons by the gold mesh could not be effectively turned into image contrast in this point-to-point imaging mode. The second phase lasts from 10 ns to about $1.2 \mu\text{s}$, featured by the intensity decreases while the surface profile of the sample remains almost unchanged, as shown in Fig. 6. With the help of scanning electron microscope, surface split along the joint of adjacent pitches on the back of the grid can be observed, indicating that there is neutral-particle ejecta in the ablation process²⁶. The last phase is from $1.2 \mu\text{s}$ to $5 \mu\text{s}$, where the intensity of melting area increases gradually. In this phase, area with intensity higher than surrounding mesh holes is considered to be melted. By compare the area size in pump-shot radiograph and that in after-shot radiograph at each time delay, melting ratio is defined as $A_{\text{pump-shot}}/A_{\text{after-shot}}$. Changing of melting ratio versus time is illustrated in Fig. 6(b), where melting ratio increases almost linearly until it approaches 1.

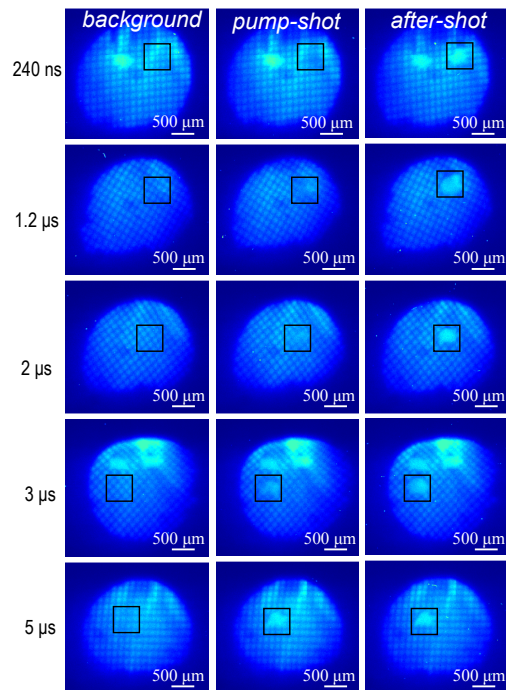


FIG. 5. Typical images of the gold mesh during the melting process. Black squares drawn in these images represent the illuminating area.

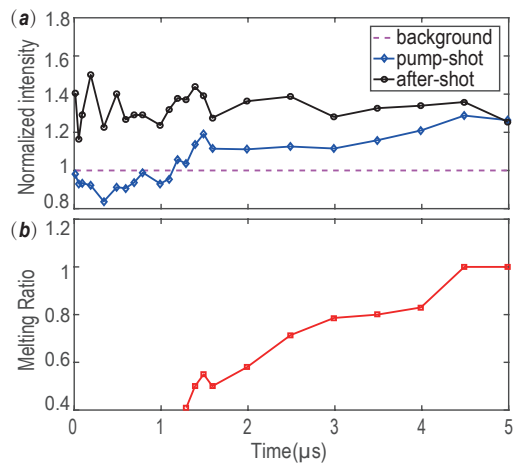


FIG. 6. Measured intensity of illuminating area (a) and melting ratio (b) at different time delays.

III. SUMMARY

In summary, dynamic high energy electron radiograph of laser-induced metal melting is demonstrated, with the combination of photo-injector generated high brightness electrons and a compact PMQ based imaging lens. With tens of ps- μm spatiotemporal resolution, dynamic high energy radiograph is proved to be suitable for high energy density matters and relevant fast dynamics processes. Moreover, spatial resolution of this dynamics HEER system can be further improved to μm level with a larger magnification factor imaging system, then more details of these dynamic processes can be observed.

IV. ACKNOWLEDGEMENT

This work was supported by the National Natural Science Foundation of China (NSFC Grant No. 11435015 and No. 11505251).

V. REFERENCES

- ¹R. P. Drake, *High-energy-density physics: fundamentals, inertial fusion, and experimental astrophysics* (Springer Science & Business Media, 2006).
- ²I. Hofmann, “Review of accelerator driven heavy ion nuclear fusion,” *Matter and Radiation at Extremes* **3**, 1–11 (2018).
- ³E. Campbell, V. Goncharov, T. Sangster, S. Regan, P. Radha, R. Betti, J. Myatt, D. Froula, M. Rosenberg, I. Igumenshchev, W. Seka, A. Solodov, A. Maximov, J. Marozas, T. Collins, D. Turnbull, F. Marshall, A. Shvydky, J. Knauer, R. McCrory, A. Sefkow, M. Hohenberger, P. Michel, T. Chapman, L. Masse, C. Goyon, S. Ross, J. Bates, M. Karasik, J. Oh, J. Weaver, A. Schmitt, K. Obenschain, S. Obenschain, S. Reyes, and B. Van Wonterghem, “Laser-direct-drive program: Promise, challenge, and path forward,” *Matter and Radiation at Extremes* **2**, 37–54 (2017).
- ⁴W. Gai, J. Qiu, and C. Jing, “Electron imaging system for ultrafast diagnostics of hdp,” in *Target Diagnostics Physics and Engineering for Inertial Confinement Fusion III*, Vol. 9211 (International Society for Optics and Photonics, 2014) p. 921104.
- ⁵C. L. Morris, N. King, K. Kwiatkowski, F. Mariam, F. Merrill, and A. Saunders, “Charged particle radiography,” *Reports on Progress in Physics* **76**, 046301 (2013).
- ⁶C. Morris, J. W. Hopson, and P. Goldstone, “Proton radiography,” *Los Alamos Science* **30**, 32 (2006).
- ⁷C. Morris, E. Ables, K. Alrick, M. Aufderheide, P. Barnes Jr, K. Buescher, D. Cagliostro, D. Clark, D. Clark, C. Espinoza, *et al.*, “Flash radiography with 24 gev/c protons,” *Journal of Applied Physics* **109**, 104905 (2011).
- ⁸N. King, E. Ables, K. Adams, K. Alrick, J. Amann, S. Balzar, P. Barnes Jr, M. Crow, S. Cushing, J. Eddleman, *et al.*, “An 800-mev proton radiography facility for dynamic experiments,” *Nuclear Instruments and Methods in Physics Research Section A: Accelerators, Spectrometers, Detectors and Associated Equipment* **424**, 84–91 (1999).
- ⁹S. Kolesnikov, A. Golubev, V. Demidov, S. Dudin, A. Kantsyrev, V. Mintsev, G. Smirnov, V. Turtikov, A. Utkin, B. Sharkov, *et al.*, “Application of charged particle beams of twac-itcp accelerator for diagnostics of high dynamic pressure processes,” *High Pressure Research* **30**, 83–87 (2010).
- ¹⁰Y. M. Antipov, A. Afonin, A. Vasilevskii, I. Gusev, V. Demyanchuk, O. Zyatkov, N. Ignashin, Y. G. Karshev, A. Larionov, A. Maksimov, *et al.*, “A radiographic facility for the 70-gev proton accelerator of the institute for high energy physics,” *Instruments and Experimental Techniques* **53**, 319–326 (2010).
- ¹¹F. Merrill, A. Golubev, F. Mariam, V. Turtikov, D. Varentsov, and H. Collaboration, “Proton microscopy at fair,” in *AIP Conference Proceedings*, Vol. 1195 (AIP, 2009) pp. 667–670.
- ¹²F. Merrill, F. Harmon, A. Hunt, F. Mariam, K. Morley, C. Morris, A. Saunders, and C. Schwartz, “Electron radiography,” *Nuclear Instruments and Methods in Physics Research Section B: Beam Interactions with Materials and Atoms* **261**, 382–386 (2007).
- ¹³Z. Zhou, Y. Du, S. Cao, Z. Zhang, W. Huang, H. Chen, R. Cheng, Z. Chi, M. Liu, X. Su, *et al.*, “Experiments on bright-field and dark-field high-energy electron imaging with thick target material,” *Physical Review Accelerators and Beams* **21**, 074701 (2018).
- ¹⁴F. Merrill, J. Goett, J. Gibbs, S. Imhoff, F. Mariam, C. Morris, L. Neukirch, J. Perry, D. Poulson, R. Simpson, *et al.*, “Demonstration of transmission high energy electron microscopy,” *Applied Physics Letters* **112**, 144103 (2018).
- ¹⁵Y. Du, L. Yan, J. Hua, Q. Du, Z. Zhang, R. Li, H. Qian, W. Huang, H. Chen, and C. Tang, “Generation of first hard x-ray pulse at tsinghua thomson scattering x-ray source,” *Review of Scientific Instruments* **84**, 053301 (2013).
- ¹⁶M. Schollmeier, S. Becker, M. Geißel, K. Flippo, A. Blažević, S. Gaillard, D. Gautier, F. Grüner, K. Harres, M. Kimmel, *et al.*, “Controlled transport and focusing of laser-accelerated protons with miniature magnetic devices,” *Physical review letters* **101**, 055004 (2008).
- ¹⁷J. Lim, P. Frigola, G. Travish, J. Rosenzweig, S. Anderson, W. Brown, J. Jacob, C. Robbins, and A. Tremaine, “Adjustable, short focal length permanent-magnet quadrupole based electron beam final focus system,” *Physical Review Special Topics-Accelerators and Beams* **8**, 072401 (2005).
- ¹⁸R. Li and P. Musumeci, “Single-shot mev transmission electron microscopy with picosecond temporal resolution,” *Physical Review Applied* **2**, 024003 (2014).
- ¹⁹D. Cesar, J. Maxson, P. Musumeci, Y. Sun, J. Harrison, P. Frigola, F. OShea, H. To, D. Alesini, and R. Li, “Demonstration of single-shot picosecond time-resolved mev electron imaging using a compact permanent magnet quadrupole based lens,” *Physical review letters* **117**, 024801 (2016).
- ²⁰K. Makino and M. Berz, “Cosy infinity version 9,” *Nuclear Instruments and Methods in Physics Research Section A: Accelerators, Spectrometers, Detectors and Associated Equipment* **558**, 346–350 (2006).

- ²¹K. Flöttmann, “Astra: A space charge tracking algorithm. users manual available at [http://www. desy. de/mpyflo](http://www.desy.de/mpyflo),” Astra dokumentation (2013).
- ²²C. Scoby, R. Li, E. Threlkeld, H. To, and P. Musumeci, “Single-shot 35 fs temporal resolution electron shadowgraphy,” Applied Physics Letters **102**, 023506 (2013).
- ²³Z. Peng-Fei, F. Fei-Chao, L. Sheng-Guang, X. Dao, Z. Jie, and C. Jian-Ming, “Time-resolved visualization of laser-induced heating of gold with mev ultrafast electron diffraction,” Chinese Physics Letters **31**, 116101 (2014).
- ²⁴L. Chen, R. Li, J. Chen, P. Zhu, F. Liu, J. Cao, Z. Sheng, and J. Zhang, “Mapping transient electric fields with picosecond electron bunches,” Proceedings of the National Academy of Sciences **112**, 14479–14483 (2015).
- ²⁵P. Zhu, Z. Zhang, L. Chen, J. Zheng, R. Li, W. Wang, J. Li, X. Wang, J. Cao, D. Qian, *et al.*, “Four-dimensional imaging of the initial stage of fast evolving plasmas,” Applied Physics Letters **97**, 211501 (2010).
- ²⁶N. Zhang, X. Zhu, J. Yang, X. Wang, and M. Wang, “Time-resolved shadowgraphs of material ejection in intense femtosecond laser ablation of aluminum,” Phys. Rev. Lett. **99**, 167602 (2007).